

TM 422
FILE NO. 11 DE 31001
NACA TM 667

TECHNICAL MEMORANDUMS

NATIONAL ADVISORY COMMITTEE FOR AERONAUTICS

NACA - TM - 667

No. 667

APPLICATION OF THE THEORY OF FREE JETS

By A. Betz and E. Petersohn

Ingenieur-Archiv, May, 1931

Washington
April, 1932

REPRODUCED BY
NATIONAL TECHNICAL
INFORMATION SERVICE
U.S. DEPARTMENT OF COMMERCE
SPRINGFIELD, VA. 22161

U.S. DEPARTMENT OF COMMERCE
National Technical Information Service

NACA TM 667

APPLICATION OF THE THEORY OF FREE JETS

National Advisory Committee for Aeronautics
Washington, DC

May 31

NOTICE

THIS DOCUMENT HAS BEEN REPRODUCED FROM THE BEST COPY FURNISHED US BY THE SPONSORING AGENCY. ALTHOUGH IT IS RECOGNIZED THAT CERTAIN PORTIONS ARE ILLEGIBLE, IT IS BEING RELEASED IN THE INTEREST OF MAKING AVAILABLE AS MUCH INFORMATION AS POSSIBLE.

APPLICATION OF THE THEORY OF FREE JETS*

By A. Betz and E. Petersohn

1. INTRODUCTION

The theory of flow of free jets goes back to Helmholtz** and Kirchhoff.*** The fundamental idea is the dead water aft a body, which in the theory is now assumed perfectly still, whereas the fluid outside of this dead water is in potential motion. At the boundary of the two zones, dead water and potential flow, the velocity varies irregularly (area of discontinuity). The dead water being at rest, the pressure within its entire zone must be constant, hence also at the boundary of the potential flow. Applied to the latter, it signifies that the velocity along the free boundary must be constant (Bernoulli's equation). Now the boundary conditions for the potential flow are:

- 1) Velocity at infinity given;
- 2) Normal component on the surface of the body equal zero;
- 3) Velocity along the free boundary constant.

Such problems are solvable at least for planar flows and have been treated quite frequently.**** But the whole theory of the so-called free jets has come seriously into disrepute for the very reason that the results are not wholly in accord with practice. To illustrate: The theory ascribes to the vertical plate, sketched in Figure 1, a drag coefficient $c_w = \frac{2\pi}{4+\pi} = 0.88$, while in reality

*"Anwendung der Theorie der freien Strahlen." Ingenieur-Archiv, May, 1931, pp. 190-211.

**Helmholtz, H. v.: Wissensch. Abh., Vol. I, p. 146, Leipzig, 1882.

***Kirchhoff, G.: Ges. Abh., p. 416, Leipzig, 1882.

****Compare Handb. d. Physik, Vol. VII, p. 57 ff.

it is about 2.0. The drag coefficient is defined by the relation

$$W = c_w \frac{\rho}{2} F v_0^2,$$

where W = drag of area F , ρ = fluid density and v_0 = velocity at infinity). The discrepancy between theory and practice is due to the fact that the areas separating the dead water from the potential flow are not stable; they dissolve into eddies and set up an intense mingling motion between the two zones. The result is that the potential flow impresses shearing forces on the dead water zone, thus creating a negative pressure in the space behind the plate, which increases the drag. Besides, the velocity in the dead water zone ceases to be zero, and even the form of the potential flow itself is materially altered owing to the other boundary conditions, particularly in its further course at some distance away from the body.

On the other hand, there are cases wherein these processes have no appreciable effect on the final results. An especially important sphere in which the theory of the free jet is applicable, is the discharge of water in air. By virtue of the great density difference of the two mediums the effect of the contiguous air on the flow of water is very small. The conditions are analogous to cavitation wherein the water flow borders on the empty spaces of the cavitation zone replete with vapor and air. Because of the ever-increasing importance of cavitation with our high-speed turbines, pumps and ship screws, we choose as the subject of our report the flow through screen-like arrangements with free jet boundaries which in a certain measure represent simplified types of the above-mentioned machines. (Figs. 3, 8, and 10.)

Aside from that, we wish to solve the problem as to what extent the results of the theory of free jets are qualified to render the actual processes of discharge of air in air or of water in water without cavitation. The break-up of the discontinuity layer into eddies occurs after all, only gradually, and actually results in free jet boundaries at the instance of separation from the body. So, when the flow aft of the body approaches asymptotically a steady state, i.e., as in Figure 2, this final attitude may already have been attained by appropriate measurement before the interferences due to instability of the jet boundaries and the interdependent mingling processes

make themselves conspicuous. It is to be expected in such cases that the formation of the areas of discontinuity follows, according to the theory, without the subsequent mingling effecting any marked change. These propitious circumstances are as a rule encountered when the areas of quiescent fluid are large compared with those of the potential flow. And the very conditions prevail for the flow through the above-mentioned screens. (Figs. 3, 8, and 10.) As long as the slots are very narrow with respect to the screen bars, a close accord between theory and practice may be expected.

But when the slots are consistently widened and so make the stationary bars narrow relative to the openings, the process with screen, according to Figure 3, for instance, manifests a steady approach toward that shown in Figure 1, where the adjacent bars are so far removed in proportion as to become negligible. Here the inadequacy of the theory is generally conceded, and the question arises as to how wide the slots can be made without bringing about appreciably erroneous theoretical values, and what other circumstances are involved. To answer this question, we compared a portion of the results arrived at according to the theory of free jets with corresponding experiments.

For the theoretical treatment we made use of Prandtl's hodograph method. This method is quite familiar to students of Prandtl, as well as to a limited circle of other professional men, but has never been fully described* as far as we know, and is therefore little known elsewhere. Hence a more detailed account may not be amiss. Compared to the other conventional methods, the hodograph is clearer and for that reason more convenient for the engineer, because it avoids many abstruse intermediate transformations. Moreover, in view of the practical importance of cavitation phenomena, an explanation of the method from the engineer's point of view seems justified.

The flow can be expressed by the complex potential function

$$\Phi = \phi + i\psi \quad (1)$$

*Brief excerpts may be found in the article "Fluid Motion," in Handwörterbuch der Naturwissenschaften, Vol. IV, p. 110, Jena, 1913, as well as in der Hütte, 25th edition, Vol. I, p. 347.

subject to the complex coordinate

$$z = x + i y$$

$$\phi = \Phi(z) \quad (3)$$

(where ϕ = flow potential, ψ = stream function, x and y = coordinates in the plane of the flow). With u and v as velocity components in direction of axis x and y , respectively, in point z , we have

$$w = u - i v = \frac{\partial \Phi}{\partial z} \quad (4)$$

This, however, is an analytical function of z , because Φ is one. So when we plot in a new representation, plane w , a point $w = u - i v$ for each point z of plane z , the lines of plane z become lines of plane w and are conformal to one another because of the analytical character of the conformal function. To illustrate, when we transfer a set of stream and potential lines ($\psi = \text{constant}$; $\phi = \text{constant}$) of plane z (plane of flow) in this manner to plane w , the result is a conformal transformation of it. This special transformation by means of velocity vector w is called "hodograph."* By conformal representation, however, a potential flow invariably changes into a potential flow again, as a result of which the group of lines obtained in plane w , may themselves be looked upon as stream and potential lines of a new flow. Now, if we succeed in grasping this new flow theoretically, that is, define Φ as function of

*The velocity vector of the flow is $w' = u + iv$, hence w is the conjugated velocity vector, or in other words, w is the reflection or image of w' on axis x . The transformation of the flow by its velocity field $w' = u + iv$ as well as its reflection by $w = u - iv$ is called hodograph. In the interest of a precise manner of expression, it would, of course, be expedient to confine the term "hodograph" to the first representation (w') and to call the other (w) the "reflected hodograph."

w ,* the solution for plane z , that is $\Phi(z)$, is as-
sured. According to equation (4)

$$w = \frac{\partial \Phi}{\partial z} \quad (5)$$

from which follows

$$z \equiv \int \frac{1}{w} d\Phi \quad (6)$$

Knowing Φ as function of w and thereby w as
function of Φ the integral may be carried through, so
that

$$z = z(\Phi) \quad (7)$$

and vice versa, $\Phi = \Phi(z) \quad (8)$

*The course of flow is, after all, qualitatively known as a rule. Hence the hodograph and the shape of the streamlines can be readily plotted in it by estimating the velocity for a suitable sequence of points on one streamline and then plot it from one point on (the origin of the coordinates of the hodograph). The pertinent end points for one and the same streamline of these velocity vectors are then connected and represent the corresponding streamline of the hodograph. The latter displays certain singular spots (mostly sources and sinks) which then serve for more exact definition of the flow in the hodograph. The frequency of the following cases is noteworthy: If the flow in the plane of flow at infinity changes into a parallel flow, the velocity for all streamlines there is of equal magnitude and unidirectional. In the hodograph the equivalent of "at infinity" is one single point into which all streamlines empty (source or sink). In the stagnation points of the plane of flow the velocity is zero. The corresponding point in the hodograph lies in the zero point. As branching point of the streamlines in the plane of flow it generally becomes branching point in the hodograph also, and likewise stagnation point.

2. THE FLAT SCREEN MOUNTED PERPENDICULAR TO THE FLOW ACCORDING TO THE THEORY*

Our examination may be confined to one strip of width a , because the flow pattern always repeats itself for each one of such strips. Besides, it is immaterial how we select the boundaries of the strip. If our choice falls on two adjacent streamlines passing through the stagnation point, as in Figure 3, the result will be as portrayed in Figure 2. In the following, we let the lines A_3D_3 and A_4D_4 represent the boundaries of the considered zone.

The pertinent flow in plane w , which resembles the flow in Figure 3, that is, the hodograph reflected in axis x , has the appearance of that of Figure 4. The heavy lines correspond to the heavily drawn (see fig. 3), rigid boundaries of Figure 3. The letters in Figures 3 and 4 designate corresponding points. Points coinciding in plane w are differentiated in the plane of the flow by arrows. We begin at point A_1 , which is situated at infinity where velocity v_1 parallel to direction x prevails. Correspondingly, point A in plane w lies on axis x at distance v_1 from the zero point. Proceeding in the plane of the flow (fig. 3) along the straight streamline A_1B , the velocity retains its direction, whereas its magnitude decreases and drops to zero in point B . Accordingly, we obtain in plane w a straight line from point A to the zero point. The latter coincides with point B , where the flow splits up. We first follow the upper branch BC_1 . The velocity increases along the boundary area BC_1 and becomes v_2 by the time it reaches the end of the area and is perpendicularly upward (positive imaginary direction). Conformably, we have in plane w a downward inclined straight line from zero point (B) (negative imaginary direction), because $w = -i v$ (reflection of velocity vector on axis x) up to point C_1 at distance v_2 from the zero point. Here is the beginning of the free jet boundary C_1D_1 (in the plane of the flow), where velocity v_2 remains constant in magnitude but varies in direction by gradually changing from vertical into horizontal. The equivalent to this in plane w is a circular arc (constant distance from zero point), extending

*Solved by R. v. Mises, V.D.I., Vol. 61, 1917, p. 447. Treated here merely as particularly simple example for introducing the hodograph method, so as to make subsequent more complicated problems easier to solve.

N.A.C.A. Technical Memorandum No. 667

from point C_1 to point D on axis x (quadrant). The bounding streamline A_3D_3 of the plane of the flow becomes the straight line AD in plane w . Following the other branch ABC_2D_2 in the same manner, we obtain in plane w the reflected contour of the one just explained, and both together form a semicircle.* All other streamlines within this boundary in the plane of the flow, begin in plane w in point A , because all have the same velocity v_1 at infinity. They all terminate in plane w in one common point D , because the terminal velocity v_2 is the same for all streamlines of the plane of the flow.

In addition, since component x of the velocity never becomes negative and the absolute value of the velocity never exceeds v_2 , the streamlines in plane w are all within the described limits; and for as much as no unsteady velocity changes occur in the plane of the flow the streamlines of plane w likewise fill the allotted space completely. The flow in plane w is now so characterized (boundary condition), that all streamlines begin in point A (source), end in point D (sink), and fills the prescribed space bounded by a semicircle and a diameter.

Withal it is provisionally undecided as yet how large the ratio v_1/v_2 , the initial to the terminal velocity, is, and by it, where point A (source) lies on BD in plane w . Obviously, this ratio is dependent upon the relative width of the slot. If the slot is as wide as the spacing, so that the plates become infinitely narrow, the flow continues without hindrance; it is $v_2 = v_1$. On the other hand, if the slot is very narrow, the free jet likewise becomes very narrow compared to the oncoming fluid flow, which has the whole width of the spacing at its disposal. Accordingly, $v_1 \ll v_2$, hence $\frac{v_1}{v_2} \rightarrow 0$. This interdependence between slot width and v_1/v_2 is not readily amenable to definition in a quantitative sense, and so it becomes an important part of this problem to determine this relationship. Since we find the processes in the plane of the flow from its image in the hodograph

*The selection of any two other congruent lines at distance a from one another instead of the straight boundary lines A_3D_3 and A_4B_4 would result in plane w , in two curves in place of the two coinciding straights AD ; but they likewise coincide because of the congruent shape of the two boundaries of the plane of flow, so that the two zones again yield a complete semicircle.

by integration (equation (6)), we expediently continue in the same fashion by first assuming point A arbitrarily in plane w (that is, v_1/v_2), and then define therefrom the slot width by integration based upon equation (6). The result is, the slot width in function of v_1/v_2 and through it, of course, also the reverse connection. The absolute magnitude of these velocities is of no significance, because a proportionate enlargement of all velocities does not alter the form of the streamlines. We may therefore, put velocity $v_2 = 1$ which, moreover, has the advantage that the limiting circle in plane w becomes precisely the unit circle. Likewise, we may, without detracting from the generality, set the spacing a in the plane of the flow $= 1$. Now the yield of the source in point A of plane w is $E = v_1$.

The flow in plane w , source and sink, within a semicircle are readily treated: First we complete the semicircle to a full circle by reflection on axis y and further on, by reflection of the inside on the periphery to the indefinitely extended plane. The result is the flow, shown in Figure 5, clearly defined by four sources and two sinks and the premises of zero at indefinite velocity. Each of the four sources has a yield v_1 and lies in the points $+v_1$, $-v_1$, $+\frac{1}{v_1}$ and $-\frac{1}{v_1}$. Each of the two sinks has the yield $-2v_1$ (by reflection on the circle to original yield is doubled) and lies in points $+1$ and -1 , respectively. The complex potential of a source (sink) in point z_0 and with a yield E is in a point z

$$\Phi = \frac{E}{2\pi} \ln(z - z_0) \quad (9)$$

We are primarily interested in the conditions on $C_1 C_2$ from which the length of the planes $C_1 C_2$ in the plane of the flow must now be derived. Our four sources ($E = v_1$) and two sinks ($E = -2v_1$) reveal for a point of this space at distance r from the zero point, that is, for a point $z = ir$,

$$\Phi = \frac{v_1}{2\pi} \left[\ln(ir - v_1) + \ln(ir + v_1) + \ln\left(ir - \frac{1}{v_1}\right) + \ln\left(ir + \frac{1}{v_1}\right) - 2 \ln(ir - 1) - 2 \ln(ir + 1) \right] \quad (10)$$

Now, when we resolve the individual logarithmic terms

(for example, $\ln \sqrt{r^2 + v^2}$) into real and imaginary parts (for example, $\arctan \frac{r}{v}$, we find that the imaginary parts exactly annul one another owing to the symmetrical position of point ir (on axis y) to the sources and sinks. Only the real parts remain. So, instead of the complex quantities Φ , w and z of equation (6), we can simply figure with the real quantities Φ , r and y . It is

$$\Phi = \varphi = \frac{v_1}{2\pi} \ln \left[(r^2 + v_1^2) \left(r^2 + \frac{1}{v_1^2} \right) \frac{1}{(r^2 + 1)^2} \right] \quad (11)$$

and

$$\frac{\partial \Phi}{\partial r} = \frac{v_1}{2\pi} 2r \left[\frac{1}{r^2 + v_1^2} + \frac{1}{r^2 + \frac{1}{v_1^2}} - \frac{2}{r^2 + 1} \right] \quad (12)$$

Now, according to (6), we obtain for a point ir on plane w , a corresponding point iy on plane of the flow

$$y = - \int_0^r \frac{1}{r} \frac{\partial \Phi}{\partial r} dr = - \frac{v_1}{\pi} \int_0^r \left[\frac{1}{r^2 + v_1^2} + \frac{1}{r^2 + \frac{1}{v_1^2}} - \frac{2}{r^2 + 1} \right] dr, \\ = - \frac{v_1}{\pi} \left[\frac{1}{v_1} \arctan \frac{r}{v_1} + v_1 \arctan v_1 r - 2 \arctan r \right] \quad (13)$$

The whole distance $C_1 C_2 = b$ (width of plate) is obtained by integration in plane w from C_1 to C_2 , that is, from $r = -1$ to $r = +1$. It affords

$$b = 2 \frac{v_1}{\pi} \left[\frac{1}{v_1} \arctan \frac{1}{v_1} + v_1 \arctan v_1 - \frac{\pi}{2} \right] \\ = 2 \frac{v_1}{\pi} \left(v_1 - \frac{1}{v_1} \right) \arctan v_1 + (1 - v_1).$$

For simplification we put $a = 1$ and $v_2 = 1$. To get rid of this standardization, we now replace b by $\frac{b}{a}$ and v_1 by $\frac{v_1}{v_2}$, so that

$$\frac{b}{a} = 1 - \frac{v_1}{v_2} - \frac{2}{\pi} \left[1 - \left(\frac{v_1}{v_2} \right)^2 \right] \arctan \frac{v_1}{v_2} \quad (14)$$

This relationship is shown in Figure 12 (curves $\alpha = 90^\circ$).

To arrive at force W impressed on each plate strip the knowledge of the initial and the terminal velocity suffices. For, according to the momentum theory,

$$W = p_1 a + \rho v_1^2 a - p_2 a - \rho v_1 v_2 a, \quad (15)$$

where p_1 and p_2 denote the pressure remotely fore and aft of the screen. Bernoulli's equation reads

$$p_1 - p_2 = \frac{\rho}{2} (v_2^2 - v_1^2) = \frac{\rho}{2} v_2^2 \left[1 - \left(\frac{v_1}{v_2} \right)^2 \right] \quad (16)$$

Consequently,

$$\begin{aligned} W &= a \frac{\rho}{2} v_2^2 \left[1 - \left(\frac{v_1}{v_2} \right)^2 - 2 \frac{v_1}{v_2} + 2 \left(\frac{v_1}{v_2} \right)^2 \right], \\ &= a \frac{\rho}{2} v_2^2 \left[1 + \left(\frac{v_1}{v_2} \right)^2 - 2 \frac{v_1}{v_2} \right] = a \frac{\rho}{2} v_2^2 \left[1 - \frac{v_1}{v_2} \right]^2 \quad (17) \end{aligned}$$

A dimensionless resistance coefficient $c_w = \frac{W}{\frac{\rho}{2} v_2^2 b}$, formed herefrom, becomes

$$c_w = \frac{a}{b} \left[1 - \left(\frac{v_1}{v_2} \right) \right]^2 \quad (18)$$

with relation (equation (14)) between $\frac{b}{a}$ and $\frac{v_1}{v_2}$. This is also shown in Figure 18 ($\alpha = 90^\circ$, $\gamma = 0^\circ$) where, however, the more general c_n is used instead of c_w . In the limiting case of $\frac{v_1}{v_2} \rightarrow 1$, that is, for one single plate in an infinitely wide flow, equation (18) reveals Kirchhoff's resistance coefficient $c_w = \frac{2\pi}{4 + \pi}$.

To gain an estimate of the rapidity with which the free jets leave the slots and approach their asymptotic terminal attitude, we examine the curves of the free jet limit itself. Its counterpart in plane w is the circular arc from C_1 to D and C_2 to D , respectively. On this circular arc

$$w = e^{i\vartheta} \quad (19)$$

when ϑ is the angle of the vector component to a point of the circular arc with axis x . In plane z we have

for these points

$$z - C_1 = \int_{C_1}^w \frac{\partial \Phi}{\partial w} \frac{1}{w} dw = \int_{-\frac{\pi}{2}}^{\vartheta} \frac{\partial \Phi}{\partial \vartheta} e^{-i\vartheta} d\vartheta \quad (20)$$

For the points of the circle, we find

$$\Phi = \frac{v_1}{2\pi} \left[\ln(e^{i\vartheta} - v_1) + \ln(e^{i\vartheta} + v_1) + \ln\left(e^{i\vartheta} - \frac{1}{v_1}\right) + \ln\left(e^{i\vartheta} + \frac{1}{v_1}\right) - 2 \ln(e^{i\vartheta} - 1) - 2 \ln(e^{i\vartheta} + 1) \right] \quad (21)$$

The imaginary portion (the stream function) either disappears or else is constant, because the circle is streamline. Besides,

$$\frac{\partial \Phi}{\partial \vartheta} = \frac{v_1}{2\pi} i e^{i\vartheta} \left[\frac{1}{e^{i\vartheta} - v_1} + \frac{1}{e^{i\vartheta} + v_1} + \frac{1}{e^{i\vartheta} - \frac{1}{v_1}} + \frac{1}{e^{i\vartheta} + \frac{1}{v_1}} - \frac{2}{e^{i\vartheta} - 1} - \frac{2}{e^{i\vartheta} + 1} \right] \quad (22)$$

Consequently, we have, according to (20),

$$z - C_1 = \frac{v_1}{2\pi} i \int_{-\frac{\pi}{2}}^{\vartheta} \left[\frac{1}{e^{i\vartheta} - v_1} + \frac{1}{e^{i\vartheta} + v_1} + \frac{1}{e^{i\vartheta} - \frac{1}{v_1}} + \frac{1}{e^{i\vartheta} + \frac{1}{v_1}} - \frac{2}{e^{i\vartheta} - 1} - \frac{2}{e^{i\vartheta} + 1} \right] d\vartheta \quad (23)$$

The integrals jointly have the form $I = \int \frac{d\vartheta}{e^{i\vartheta} + k}$ which, when resolved into real and imaginary part, becomes:

$$\begin{aligned} I &= \int \frac{(k + \cos \vartheta) d\vartheta}{1 + k^2 + 2k \cos \vartheta} - i \int \frac{\sin \vartheta d\vartheta}{1 + k^2 + 2k \cos \vartheta} \\ &= \frac{1}{2k} \left[\vartheta - 2 \arctan \left(\frac{1-k}{1+k} \tan \frac{\vartheta}{2} \right) + i \ln(1 + k^2 + 2k \cos \vartheta) \right] \quad (24) \end{aligned}$$

Introduction of this result into (23), whereby k assumes for the individual integral, in sequence, the values $-v_1$, $+v_1$, $-\frac{1}{v_1}$, $+\frac{1}{v_1}$, -1 , $+1$, yields

$$z - C_1 = \frac{v_1}{2\pi} \left[\ln \frac{1 + \cos \vartheta}{1 - \cos \vartheta} - \frac{1}{2} \left(\frac{1}{v_1} + v_1 \right) \ln \frac{1 + v_1^2 + 2v_1 \cos \vartheta}{1 + v_1^2 - 2v_1 \cos \vartheta} \right] \\ + \frac{i}{2\pi} \left(\frac{1}{v_1} - v_1 \right) \left[\arctan \frac{2v_1}{1 - v_1^2} - \arctan \frac{2v_1}{1 - v_1^2} \sin \vartheta \right] \quad (25)$$

The real portion of this term represents the x coordinates, the imaginary part the y coordinates of the free jet limit in the plane of flow, figured from point C_1 . The course of the free jet limits obtained in this manner, is illustrated in Figures 6 and 7 for several values of v_1 and v_1/v_2 . The screen spacing a , in Figure 6, was kept constant, whereas the bar width b was varied. In Figure 7 the bar width was constant and the screen spacing a , was changed.

3. THE SCREEN CONSISTING OF OBLIQUE FLAT PLATES IN PERPENDICULAR FLOW, ACCORDING TO THE THEORY

We again proceed with screen spacing $a = 1$ and terminal velocity of free jets $v_2 = 1$, and review the phenomena in a strip of the width of screen spacing a . First we examine the streamline containing the stagnation point on the plates ($w = 0$). Now this line is no longer straight, as in the preceding case, hence its reflection in plane w is curved also. Figure 8 gives the approximate course of the flow and Figure 9, the singularities of the accompanying hodograph (plane w) reflected on axis x . Corresponding points are again designated by the same letters. In the previous case the initial velocity v_1 was at first undefined and its relation to given dimensions of the plates was established later. Now, we have, in addition, another temporarily undetermined quantity, namely, the direction of the terminal velocity v_2 , which is chiefly dependent on the setting of the plates. To be sure, the direction BA is given in the hodograph by point A (source), but the distance from B is indefinite and as far as point D (sink) is concerned, we know it does lie on the unit circle but not at that place. The first uncertainty is temporarily left as it is, i. e., we select point A arbitrarily on the part of axis x within the unit circle. The location of point D (the sink) is defined by the stipulation that point B , the stagnation point in plane w , must coincide with the zero

point.* This is possible only by a well-defined location of the sink, when that of the source is given.** Since a source of yield E , whose distance w from zero point forms angle χ with the plate given in zero point a velocity component $\frac{E}{2\pi w} \cos \chi$ parallel to the plate (the components normal to plate are annulled by reflection), and the sum of the effects of all sources is to be zero, we obtain as condition for angle β formed by vector BD and axis x :

$$2 \cos(\alpha - \beta) = \left(v_1 + \frac{1}{v_1}\right) \cos \alpha, \quad (26)$$

where α is the angle of the plates and β the angle of the free jets at infinity with axis x .

The hodograph for this generalized case comprises, as before, a semicircle with one source and one sink (not symmetrical, however). The sink lies again on the periphery, the source on a point of axis x . The yield of source and sink is $E = v_1$. After completion of the semicircle to the full plane by reflection, as in the previous example, we again obtain a flow consisting of superposed four sources and two sinks. (Fig. 9.) The source yield is $E = v_1$, the location is in points $v_1, v_1 e^{2i\alpha}, 1/v_1, (1/v_1) e^{2i\alpha}$. The two sinks have the yield $E = -2v_1$ and lie in points $e^{i\beta}$ and $e^{i(2\alpha-\beta)}$. With the potential on the diameter $C_1 C_2$, the imaginary portion disappears again for reasons of symmetry. For a point on $C_1 C_2$ at distance r from zero point ($w = r e^{i\alpha}$) we have:

$$\Phi = \varphi = \frac{v_1}{2\pi} \ln \left\{ [r^2 + v_1^2 - 2rv_1 \cos \alpha] \left[r^2 + \frac{1}{v_1^2} - \frac{2r}{v_1} \cos \alpha \right] \times [r^2 + 1 - 2r \cos(\alpha - \beta)]^{-2} \right\} \quad (27)$$

and

$$\frac{\partial \varphi}{\partial r} = \frac{v_1}{\pi} \left[\frac{r - v_1 \cos \alpha}{r^2 + v_1^2 - 2r v_1 \cos \alpha} + \frac{r - \frac{1}{v_1} \cos \alpha}{r^2 + \frac{1}{v_1^2} - 2 \frac{r}{v_1} \cos \alpha} - 2 \frac{r - \cos(\alpha - \beta)}{r^2 + 1 - 2r \cos(\alpha - \beta)} \right] \quad (28)$$

*See footnote, page 5.

**See page 14.

Accordingly, width b of the screen plate becomes, according to (6)

$$b = \int_{-1}^1 \frac{1}{r} \frac{\partial \varphi}{\partial r} dr$$

Now we introduce $\frac{\partial \varphi}{\partial r}$ from (28), evaluate the integral, apply arbitrary spacing a , and terminal velocity v_2 , so that,

$$\frac{b}{a} = \frac{1}{\pi} \frac{v_1}{v_2} \left[\frac{\cos \alpha}{2} \left(\frac{v_1}{v_2} + \frac{v_2}{v_1} \right) \ln \frac{1 - 2 \left(\frac{v_1}{v_2} \right) \cos \alpha + \left(\frac{v_1}{v_2} \right)^2}{1 + 2 \left(\frac{v_1}{v_2} \right) \cos \alpha + \left(\frac{v_1}{v_2} \right)^2} - \cos(\alpha - \beta) \ln \frac{1 - \cos(\alpha - \beta)}{1 + \cos(\alpha - \beta)} \right]$$

$$+ \left(\frac{v_1}{v_2} - \frac{v_2}{v_1} \right) \sin \alpha \left[\operatorname{arc} \tan \left(2 \frac{v_1 v_2}{v_2^2 - v_1^2} \sin \alpha \right) + \pi \left(\frac{v_2}{v_1} \right) \sin \alpha - \pi \sin(\alpha - \beta) \right] \quad (29)$$

wherein $2 \cos(\alpha - \beta) = \left(\frac{v_1}{v_2} + \frac{v_2}{v_1} \right) \cos \alpha$, according to (26).

With this last relation, (29) now becomes:

$$\frac{b}{a} = \frac{1}{\pi} \frac{v_1}{v_2} \left[\cos(\alpha - \beta) \ln \left(\frac{1 + \cos(\alpha - \beta)}{1 - \cos(\alpha - \beta)} \frac{\cos(\alpha - \beta) - \cos^2 \alpha}{\cos(\alpha - \beta) + \cos^2 \alpha} \right) + \left(\frac{v_1}{v_2} - \frac{v_2}{v_1} \right) \sin \alpha \operatorname{arc} \tan \left(2 \frac{v_1 v_2}{v_2^2 - v_1^2} \sin \alpha \right) + \pi \left(\frac{v_2}{v_1} \sin \alpha - \sin(\alpha - \beta) \right) \right] \quad (29a)$$

Equations (26), (29) and (29a) reveal the relation between the relative bar width b/a , the angle of deflection β , and the velocity ratio v_1/v_2 . Figures 12 and 15 exhibit the values for v_1/v_2 and β at $\alpha = 15^\circ$, 30° , and 60° plotted against b/a .

The forces N impressed on the individual plates must be vertical to the plate surface. Their components N_x and N_y , according to the momentum theory, are:

Footnote from page 13.

**One may instead determine the direction of terminal velocity v_2 from the condition that the force on the individual plates - according to the momentum theorem - must be normal to the surface of the plate.

$$N_x = \rho v_1 a (v_1 - v_2 \cos \beta) + a(p_1 - p_2) \quad (30)$$

whereby $p_1 - p_2 = \frac{\rho}{2}(v_2^2 - v_1^2)$;

$$N_y = \rho v_1 a v_2 \sin \beta \quad (31)$$

It is readily proved that $\frac{N_x}{N_y} = \tan \alpha$, that is, the force perpendicular to the plates, when putting

$$2 \cos(\alpha - \beta) = \left(\frac{v_2}{v_1} + \frac{v_1}{v_2} \right) \cos \alpha$$

according to (26). For this equation precisely expresses the condition that the force must be perpendicular to the plates.*

The resultant force is revealed as

$$N = \frac{N_y}{\cos \alpha} = \rho v_1 v_2 a \frac{\sin \beta}{\cos \alpha} \quad (32)$$

The dimensionless coefficient of this force becomes:

$$c_n = \frac{N}{\frac{\rho}{2} v_2^2 b} = 2 \frac{a}{b} \frac{v_1}{v_2} \frac{\sin \beta}{\cos \alpha} \quad (33)$$

and is shown in Figure 18 (curves $\gamma = 0^\circ$) for various values of α plotted against b/a .

Allowing $\frac{b}{a} \rightarrow 0$, results in the force for the individual flat plate at angle of setting α . The execution of this limiting transfer, wherein $\beta \rightarrow 0$ and $\frac{v_1}{v_2} \rightarrow 1$, yields

$$c_n = \frac{2 \pi \sin \alpha}{4 + \pi \sin \alpha}, \quad (34)$$

a factor defined direct by Lord Rayleigh.

*Compare footnote, page 14.

4. SCREEN CONSISTING OF OBLIQUE FLAT PLATES IN OBLIQUE FLOW (ACCORDING TO THEORY)

Here we have, aside from the constants of the preceding problem, the angle α formed by the direction of the oncoming flow with the normal to the plane of the screen. For the rest the designations remain the same. (Fig. 10.)

Plotting the hodograph again in the usual manner, we first notice that point A in the hodograph is no longer on axis x , but on a straight line sloping toward it at angle γ . (Fig. 11.) For the calculation itself this would imply but a very trifling change, which would not justify a separate treatment of the two cases were it not for another extremely serious difference. In the plane of flow the process in direction y is periodic. Points shifted in direction y (parallel to plane of screen) by spacing a , have the same velocity, hence coincide in the hodograph, as points P_3 and P_4 , for instance. Assuming a simple source in point A of the hodograph, as heretofore, reveals the same potential for the coinciding points P_3 and P_4 . But in the plane of the flow these points obviously have a different potential; for the lines of constant potential are perpendicular to the streamlines, and it is manifest that points P_4 and P_3' have the same potential; that, in fact, the potential in P_3 must be greater. Applying this stipulation at so great a distance in front of the screen that the flow can be considered as undisturbed, the distance $P_3' P_3 = a \sin \gamma$ and the potential difference between P_3 and P_3' , or what is the same, between P_3 and P_4 , is

$$\Delta \varphi = v_1 a \sin \gamma.$$

Proceeding in the plane of the flow from point P_4 toward point P_3 , the potential increases by the amount $\Delta \varphi$. In the hodograph one single turn around point A corresponds to the space from P_4 to P_3 . If herein the potential is to increase by $\Delta \varphi$, a vortex of circulation

$$\Gamma = \Delta \varphi = v_1 a \sin \gamma \quad (35)$$

must be at hand in point A. So aside from the source with intensity

$$E = v_1 a \cos \gamma, \quad (36)$$

a vortex of the mentioned intensity must be introduced in point A. The complex potential of a vortex of circulation Γ in point z_0 is in a point z (see equation (9))

$$\Phi = -i \frac{\Gamma}{2\pi} \ln(z - z_0) \quad (37)$$

To those readers who have some practice in conformal representation, the appearance of this vortex may, moreover, be clear, since by the representation of a simple periodic flow pattern, the components of the velocity at infinity, which is perpendicular, respectively, parallel to the direction of the periods, appear as source and sink.

Strictly, a vortex of intensity $v_1 \alpha \cos(\gamma - \beta)$ should be introduced in point D, (the sink) also. But by supplementing the flow through reflection on the circle (1st problem) the reflected circle has the opposite sense of rotation, and since both coincide, the vortices annul one another.

The stipulation, as in (26), of a stagnation point in the zero point of the hodograph (i.e., resultant force perpendicular to plate surface) affords here the relation:

$$2 \cos(\alpha - \beta) = \left(\frac{1}{v_1} + v_1\right) \cos \alpha + \left(\frac{1}{v_1} - v_1\right) \sin \alpha \tan \gamma \quad (38)$$

Thus, a calculation of the potential on line $C_1 C_2$ in the same manner as before, yields a proportion

$$\varphi_Q = \frac{v_1 \cos \gamma}{2 \pi} \ln \left\{ [r^2 + v_1 - 2rv_1 \cos \alpha] \left[r^2 + \frac{1}{v_1^2} - \frac{2r}{v_1} \cos \alpha \right] [r^2 + 1 - 2r \cos(\alpha - \beta)]^{-2} \right\}, \quad (39)$$

attributable to the sources and sinks and whose sole difference from the value in the preceding problem is the factor $\cos \gamma$.

But to this we must add the proportion of the vortices

$$\varphi_W = - \frac{v_1 \sin \gamma}{\pi} \left[\arctan \frac{r - v_1 \cos \alpha}{v_1 \sin \alpha} - \arctan \frac{r - \frac{1}{v_1} \cos \alpha}{\frac{1}{v_1} \sin \alpha} \right] \quad (40)$$

Conformable to (6), the plate width b is:

$$b = \int_{-1}^1 \frac{1}{r} \frac{\partial \phi_Q}{\partial r} dr + \int_{-1}^1 \frac{1}{r} \frac{\partial \phi_W}{\partial r} dr \quad (41)$$

The first of the two integrals up to $\cos \gamma$ is identical again with that evaluated in (26). For the second, we have:

$$\frac{\partial \phi_W}{\partial r} = - \frac{v_1 \sin \gamma \sin \alpha}{\pi} \left[\frac{v_1}{r^2 + v_1^2 - 2rv_1 \cos \alpha} - \frac{1}{v_1 \left(\frac{1}{v_1^2} + r^2 - \frac{2r \cos \alpha}{v_1} \right)} \right]$$

and

$$\begin{aligned} & \int_{-1}^1 \frac{1}{r} \frac{\partial \phi_W}{\partial r} = \frac{v_1 \sin \gamma \sin \alpha}{\pi} \\ & \times \left[\left(\frac{v_1}{v_1} - \frac{1}{v_1} \right) \frac{1}{2} \ln \frac{1 + 2v_1 \cos \alpha + v_1^2}{1 - 2v_1 \cos \alpha + v_1^2} \right. \\ & \left. + \left(\frac{1}{v_1} + v_1 \right) \cot \alpha \arctan \frac{2v_1 \sin \alpha}{1 - v_1^2} - \frac{\pi}{v_1} \cot \alpha \right] \quad (42) \end{aligned}$$

So when we discard the standardization and replace b and v_1 by b/a and v_1/v_2 , respectively, we at last obtain:

$$\begin{aligned} \frac{b}{a} &= \frac{1}{\pi} \frac{v_1}{v_2} \cos \gamma \left[\cos(\alpha - \beta) \ln \frac{1 + \cos(\alpha - \beta)}{1 - \cos(\alpha - \beta)} \right. \\ &+ \frac{\cos \alpha}{2} \left(\frac{v_1}{v_2} + \frac{v_2}{v_1} \right) \ln \frac{1 - 2 \left(\frac{v_1}{v_2} \right) \cos \alpha + \left(\frac{v_1}{v_2} \right)^2}{1 + 2 \left(\frac{v_1}{v_2} \right) \cos \alpha + \left(\frac{v_1}{v_2} \right)^2} \\ &+ \pi \left(\frac{v_2}{v_1} \sin \alpha - \sin(\alpha - \beta) \right) + \left(\frac{v_1}{v_2} - \frac{v_2}{v_1} \right) \sin \alpha \arctan \left(2 \frac{v_1 v_2}{v_2^2 - v_1^2} \sin \alpha \right) \\ &+ \frac{1}{\pi} \frac{v_1}{v_2} \sin \gamma \left[\frac{\sin \alpha \left(\frac{v_1}{v_2} - \frac{v_2}{v_1} \right)}{2} \ln \frac{1 + 2 \left(\frac{v_1}{v_2} \right) \cos \alpha + \left(\frac{v_1}{v_2} \right)^2}{1 - 2 \left(\frac{v_1}{v_2} \right) \cos \alpha + \left(\frac{v_1}{v_2} \right)^2} \right. \\ &\left. + \left(\frac{v_1}{v_2} + \frac{v_2}{v_1} \right) \cos \alpha \arctan \left(\frac{2 v_1 v_2}{v_2^2 - v_1^2} \sin \alpha \right) - \frac{v_2}{v_1} \pi \cos \alpha \right] \quad (43) \end{aligned}$$

Thereby $2 \cos(\alpha - \beta) = \frac{v_1}{v_2} + \frac{v_2}{v_1} \cos \alpha + \frac{v_2}{v_1} - \frac{v_1}{v_2} \sin \alpha \tan \gamma$, according to (38), and by applying this relation (43) now assumes the following form:

$$\frac{b}{a} = \frac{1}{\pi} \frac{v_1}{v_2} \left[\cos \gamma \cos(\alpha - \beta) \ln \left\{ \frac{1 + \cos(\alpha - \beta)}{1 - \cos(\alpha - \beta)} \frac{1 + 2 \left(\frac{v_1}{v_2} \right) \cos \alpha + \left(\frac{v_1}{v_2} \right)^2}{1 + 2 \left(\frac{v_1}{v_2} \right) \cos \alpha + \left(\frac{v_1}{v_2} \right)^2} \right\} \right. \\ \left. + \left\{ \frac{v_1}{v_2} \sin(\alpha + \gamma) - \frac{v_2}{v_1} \sin(\alpha - \gamma) \right\} \arctan \left(2 \frac{v_1 v_2}{v_2^2 - v_1^2} \sin \alpha \right) \right. \\ \left. + \pi \cos \gamma \left\{ \frac{v_2}{v_1} \sin \alpha - \sin(\alpha - \beta) \right\} - \cos \alpha \sin \gamma \right] \quad (43a)$$

The distance of stagnation point B from plate edge C_1 is manifested as

$$b_1 = \int_{-1}^0 \frac{1}{r} \frac{\partial \Phi}{\partial r} dr \\ = \frac{a}{\pi} \frac{v_1}{v_2} \left[\cos \gamma \cos(\alpha - \beta) \ln \frac{2(1 + \cos \alpha)}{1 + \left(\frac{v_1}{v_2} \right) \cos \alpha + \left(\frac{v_1}{v_2} \right)^2} - \frac{v_2}{v_1} \cos(\alpha - \gamma) \ln \frac{v_1}{v_2} \right. \\ \left. + \left\{ 2 \sin(\alpha - \beta) - \frac{v_1}{v_2} \sin(\alpha - \gamma) - \frac{v_2}{v_1} \sin(\alpha + \gamma) \right\} \arctan \frac{\sin \alpha}{1 + \cos \alpha} \right] \quad (44)$$

Thus we see in Figures 13 and 14, v_1/v_2 , and in Figures 16 and 17 the deflection angle β plotted against b/a for $\gamma = 30^\circ$ and $\gamma = 60^\circ$

The forces N acting on the individual plates again are perpendicular to the plate surface, and their magnitude is again revealed by the momentum theory as

$$N = \rho v_1 a \frac{\cos \gamma}{\cos(\alpha - \gamma)} [v_1 \sin \gamma + v_2 \sin(\beta - \gamma)] \quad (45)$$

The dimensionless coefficient of this force is

$$c_n = \frac{N}{\frac{\rho}{2} v_2^2 b} = 2 \frac{a}{b} \frac{v_1}{v_2} \frac{\cos \gamma}{\cos(\alpha - \gamma)} \left[\frac{v_1}{v_2} \sin \gamma + \sin(\beta - \gamma) \right] \quad (46)$$

These values are plotted in Figure 18 for $\gamma = 30^\circ$ and 60° conjointly with those for $\gamma = 0^\circ$.

5. CHECK OF THE THEORETICAL RESULTS BY EXPERIMENTS

From the foregoing discussion it is seen that a theoretical treatment of the flow through screens by formation of free jets is not beset by insuperable obstacles nor very much restricted in scope. But from the practical point of view it is of the utmost importance to know in what cases the theory supplies correct results and in which cases it does not. To ascertain this by experiments constituted an essential part of our problem. In making the experiments we encountered certain fundamental obstacles, which must be clearly understood, because they quite often play a role in the practical application also.

When discharging water through the screen in air the ensuing jets, as stated in the introduction, are very little affected by the surrounding air. The premises of the theory then are fairly well complied with and the experimental values show ordinarily a quite close accord with those of the theory. With discharge of water under water by cavitation the conditions are probably analogous. But in a discharge of water under water without cavitation or of air in air, a gradual mingling of the jets with the quiescent fluid sets in at the limit of the formed free jets. This mingling is accompanied by mutual forces which can exert a marked bearing on the motion of the jets as well as on the fluid around it.

The theory stipulates a plane flow, i. e., screen surfaces of indefinite length. In addition, it presupposes an indefinite series of screen bars. These two assumptions are impossible to realize by experiment, which must be made with air or water of finite sectional dimensions. After all, by discharge of water in air this is rather unessential, because each jet moves practically undisturbed through the surrounding air and for that reason is largely unaffected by the adjacent jets separated from it by air. The discharge of air in air or water in water calls for fixed walls (continuation by reflection on the fixed walls)

instead of the continuation of the flow. In other words, the fluid stream must be conducted in a fixed channel. If the screen deflects the jets, the direction of the guide channel must be so essayed that it harmonizes with the direction of the jets. Deviations from the right direction are readily recognized from the uneven pressures at the corresponding points of the two lateral channel walls.

Hereby the following disturbing phenomenon becomes conspicuous. The free jets gradually mingle with the surrounding dead water as a result of which the pressure rises. This pressure rise is dependent upon the ratio of jet width to dead water width. Under certain hypotheses a reduction in dead water width is accompanied by an increment in pressure rise which, however, is followed by instability of the jets. For if in these cases the spacing a between two jets is accidentally narrower than that of the adjacent jets, the negative pressure aft of the respective screen surface is less than aft of the adjacent one, because the pressure in the final attitude is constant and the pressure rise greater. The result is that the two jets, which "per se" are already closer to one another, incline toward one another, and so approach one another still more, because of the greater negative pressure of dead water between them. Due to this instability the jets have, under the conditions pointed out, a tendency of clinging to one side of the channel wall.

The instability can be reduced by joining the dead water spaces aft of the individual screen bars through openings in the channel walls to one common connecting channel, and thus equalizing the pressure of the individual dead spaces. However, the pressure equilibrium is not complete, particularly when the screen spacing is close compared to the length of the bars, i.e., long and narrow dead air spaces. This is truer the closer the experiment approaches the theoretical basis of the plane flow. It may appear fitting to omit the limiting walls (the guide channel) altogether aft of the screen and relinquish the simulation of plane flow. But even then, irregular mingling processes persist; especially the two boundary jets act differently from those in the center. One efficient way of stabilization consists in mounting auxiliary walls behind each bar of the screen (fig. 27d) an expedient which, however, can be applied conveniently only to flat screen and perpendicular flow.

Because of the time and cost involved, the experiments could not be carried on indefinitely, and so we selected various typical cases. The change in b/a was largely accomplished by the repeated use of the same screen bars installed in different numbers into the channel of given breadth.

The set-up for discharge of water in air is shown in Figure 19. The water is conveyed from a pressure tank through the screen without further guiding aft of the screen. Short end plates E were attached at the ends of the screen bar G in order to prevent transverse flow, which otherwise occurs under the influence of the pronounced pressure differences at the jet boundaries. We measured the pressure p_1 in front of the screen and the volume of discharge. The pressure behind the screen agrees with the air pressure in the experiment chamber. The volume of flow was defined by computing the amount of water flowing into a receptacle within a given time period. The results (dots) together with those of the theory (curves) may be seen in Figure 20. The agreement between theory and experiment is quite close, except in very extreme cases. Flat screens in perpendicular flow manifest no perceptible discrepancies from the theory until the ratio of plate width b to screen spacing a is less than 0.2. Probably the ventilation in the small space back of the bars is no longer sufficient. If such is the case, the deviation would not only be dependent upon the ratio b/a but on the ratio of bar width b to bar length also. Since this was not changed in our tests with water, our opinions are held in abeyance.

With the screen consisting of flat, oblique plates in perpendicular flow, the agreement for a mean bar width $b = 0.6 a$ (fig. 21) is passably close in deflection angle β as well as in velocity ratio v_1/v_2 . The latter shows a slight deviation at $\alpha = 60^\circ$ setting. The deviations become markedly greater as soon as bar width b exceeds the spacing a . (Fig. 22, $\frac{b}{a} = 1.2$.)

For the experiments with air we generally used a larger screen than for the tests with water. (Fig. 23.) However, in order to obtain a reliable comparison with the water experiments, we also made several tests with the same screen employed for our water tests (called "small screen" in the plots). The volume of flow here was arrived at by measuring the pressure drop in the nozzle.

before the screen ($p_0 - p_1$, fig. 23). As pressure behind the screen, we measured p_2 in the equalizing chamber connecting with the dead air spaces.

The results of our tests with air are shown in Figures 24-26. The flat screen in perpendicular flow reveals for large values of b/a , that is, narrow slits with large dead air spaces between, a tolerably close accord. (See I, Introduction, page 1.) The deviations, however, begin sooner and exceed those of the water experiments. Subsequently, we shall refer to this again, and for that reason, we show in Figure 24 only the results with the small screen (also used for water tests) and for free extension only. The unsymmetrical arrangements reveal decidedly greater deviation from the theory. The interaction of the jet plainly sets up an additional negative pressure on the dead water existing between free jet and plate, which sucks the jet toward the plate and effects a greater deflection β in consequence.

Now in order to explain the processes which cause this variance with the theory somewhat more clearly, we made some further tests with the flat screen in a perpendicular flow. The various set-ups (a with channel guide, b free discharge, c with end plates, d with channel guide and intermediate bars) can be seen in Figure 27. Two sizes (15 mm and 30 mm width) of screen bars were used.

The results of the pressure readings under the different test conditions are given in Figures 28 and 29. But in interpreting these data it should be noted that in part they are quite uncertain for a repetition of the tests revealed marked differences often for no clearly visible reason. As one instance of this, we reproduced the two curves for set-up b as obtained at different times. The processes really are very unstable in part, so that minor influences may have comparatively great effects. For that reason our intention is not to draw too far-reaching conclusions from the results of this test program. Nevertheless, we believe to find certain guiding points confirmed by our tests. The use of the guide channel with equalizing chamber* and the free discharge with end plates evoked a

*In these experiments equalizing chambers were used at both ends of the bars, interconnected by rubber hose (fig. 27a). In the previously described tests we used only one such chamber at one end (fig. 23).

marked difference for the two plate widths; with the narrow plates the discrepancy is decidedly higher. Apparently the ratio of plate length to plate width (200 : 15) is too high to ensure a sufficiently abundant ventilation of the dead air spaces back of the plates. The effect of the above-mentioned intermediate bars behind the separate plates is astonishing (fig. 27d); the values are in close accord with the theoretical curve for both narrow and wide plates.

For a better insight into the causes of the different results we measured in some of the set-ups of Figure 27 the velocity (energy) distribution (total pressure) 13 cm aft of the plate (line A-A in figs. 27a and 27d). The results are given in Figure 30. It is clearly seen that the mingling process in the individual jets is very different. It is also manifest, even if not quite as noticeable, that the jets do not run parallel while the distances of the maxima and minima are uneven. The bar behind each screen plate makes the movement of the jets much more uniform. It may in part be due to better "guidance" of the jets, thus making them independent of one another. But in the main this greater uniformity undoubtedly is due to the fact that now each jet is bounded by a fixed wall for at least a distance, and that as a result thereof the difference between the outside and inside jets is reduced.

In order to be independent of the mutual interference of the jets, we further examined one single slot (corresponding to fig. 3), first with continuation of channel and then without channel and with and without end plates. (Fig. 31.) The result is appended in Figure 32. With and without channel but with end plates, the results showed the deviations from the theory to be quite inferior, as expected, by the satisfactory ventilation of the dead air zones. The greatest variation occurred at the jet ends in absence of guidance. Manifestly, transverse movements appearing at these places exert a quite pronounced effect. (Compare fig. 28.)

6. SUMMARY

Based upon Kirchhoff's theory of free jets the flow through different screen arrangements of flat plates, as chiefly encountered with turbines in the cavitation zone is defined. It is shown by experiments that these the-

retical results are very well representative in most cases of the conditions of discharge from water in air and consequently by cavitation. In addition, the experiments reveal a picture of the discrepancies between the actual flow and the theory of discharge of air in air (of water in water without cavitation). These discrepancies are explained qualitatively by the mingling processes between the jets and the dead air zones.

Translation by J. Vanier,
National Advisory Committee
for Aeronautics.

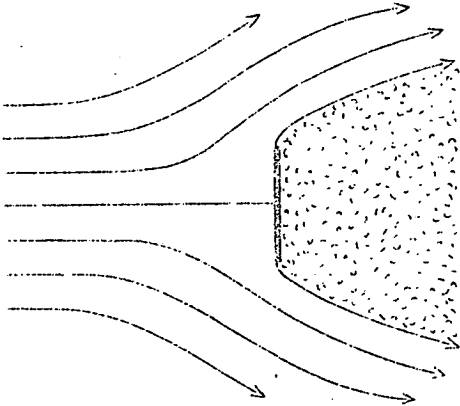


Fig. 1 Kirchhoff's flow around a plate.

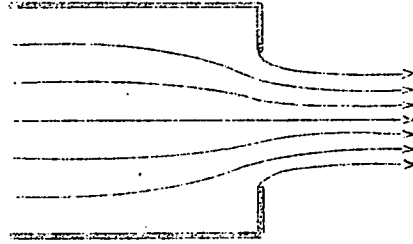


Fig. 2 Discharge from a receptacle.

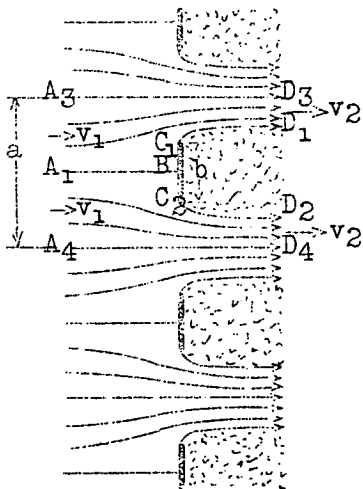


Fig. 3 Flow through a screen.

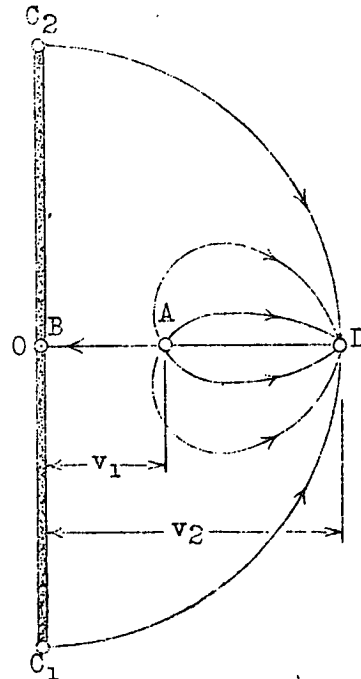


Fig. 4 Reflected hodograph to flow according to figure 3.

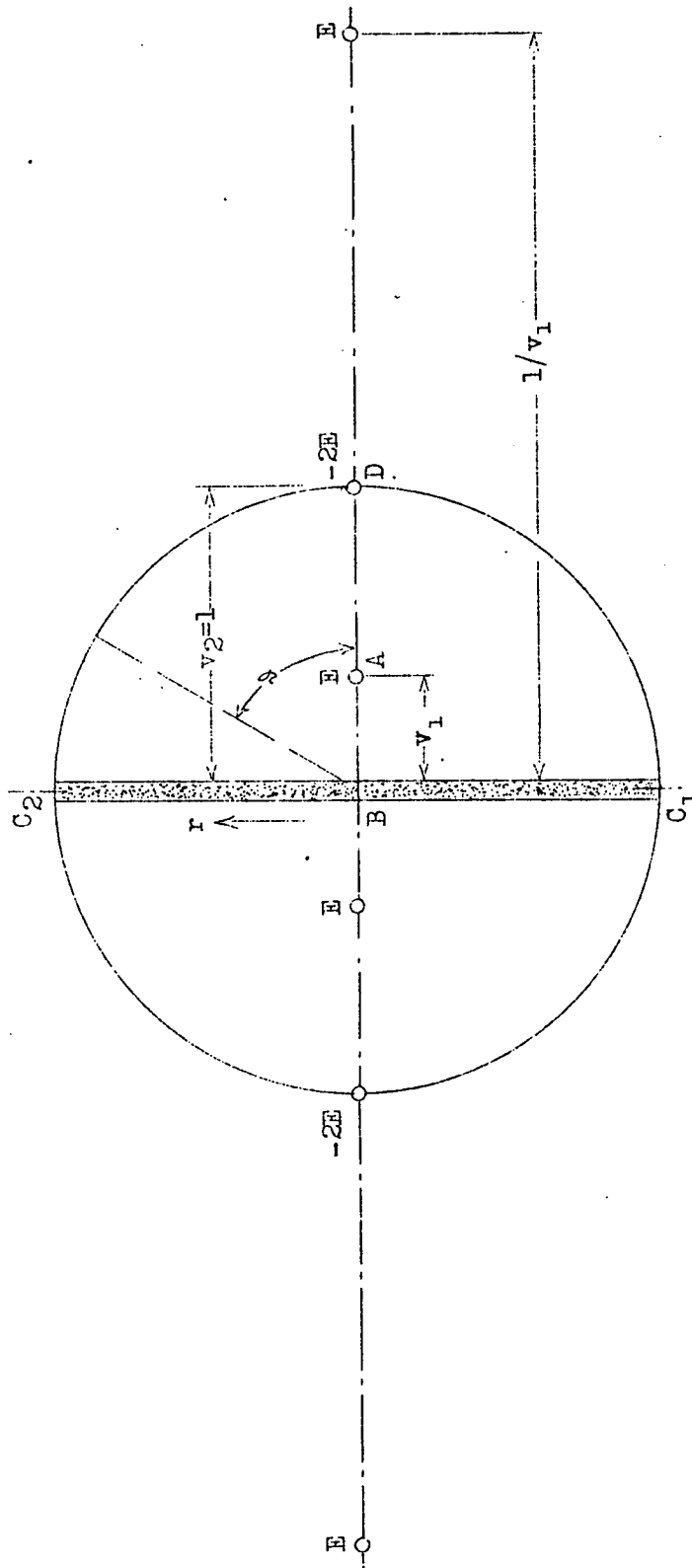


Fig.5 Phenomena of hodograph flow.

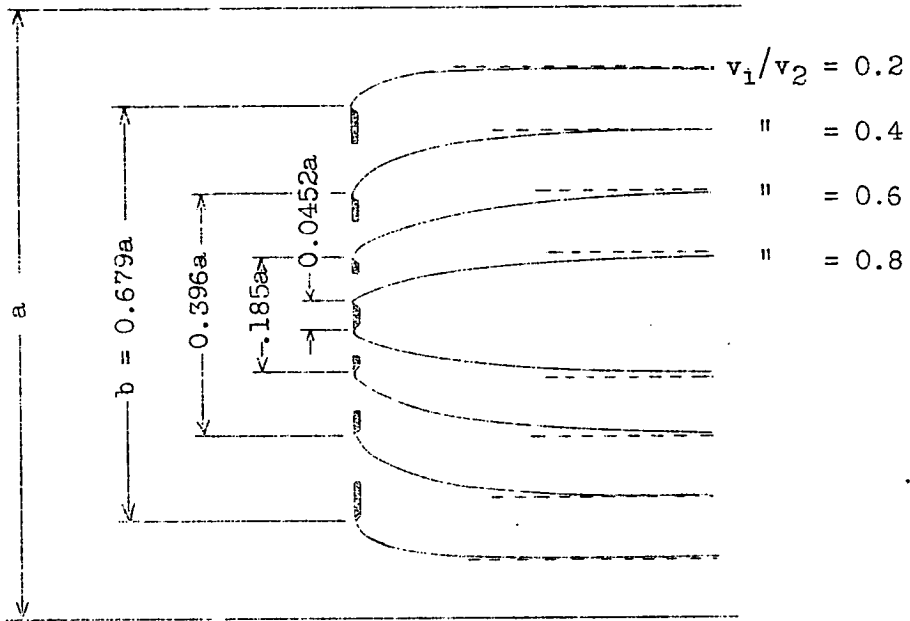


Fig.6 Dead air boundaries behind screen bars of different width by equal screen spacing.

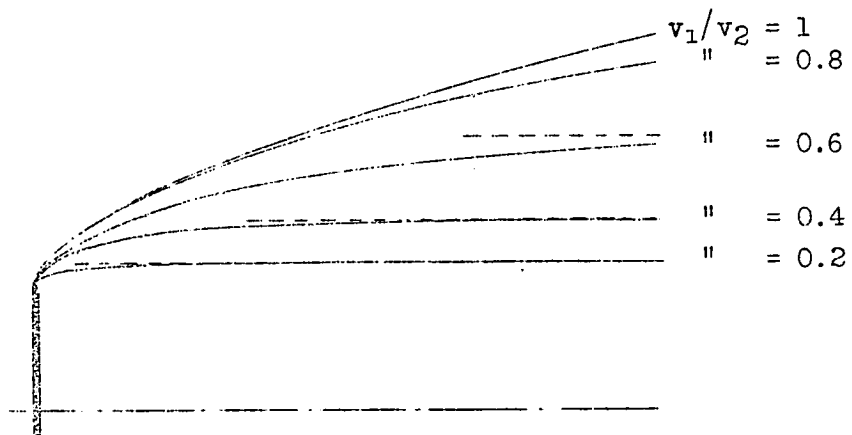


Fig.7 Dead air limits behind screen bars of equal width by different screen spacing.

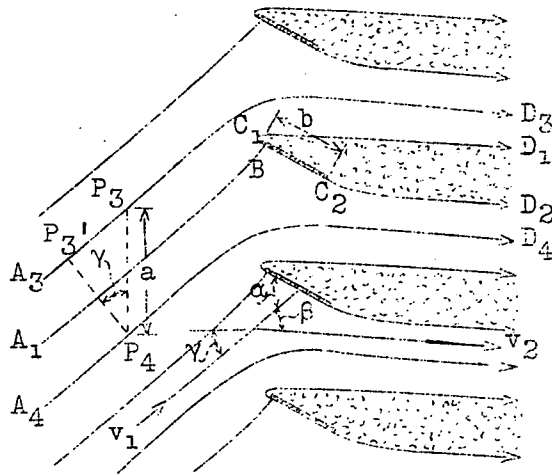


Fig.10 Screen of oblique plates in oblique flow.

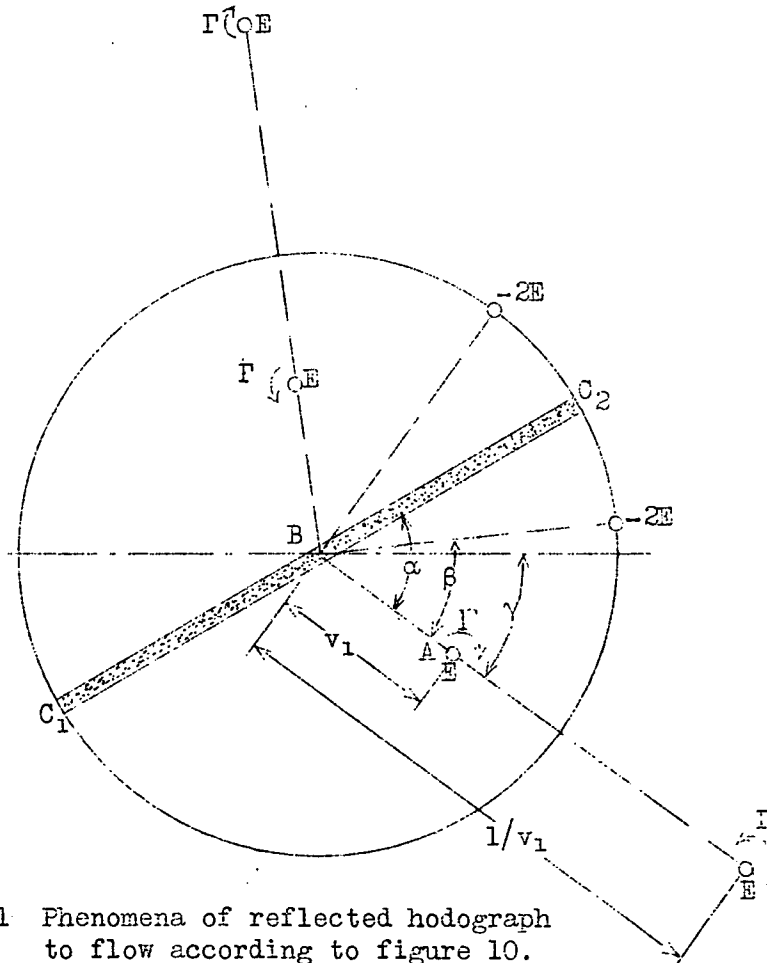


Fig.11 Phenomena of reflected hodograph to flow according to figure 10.

Fig.12

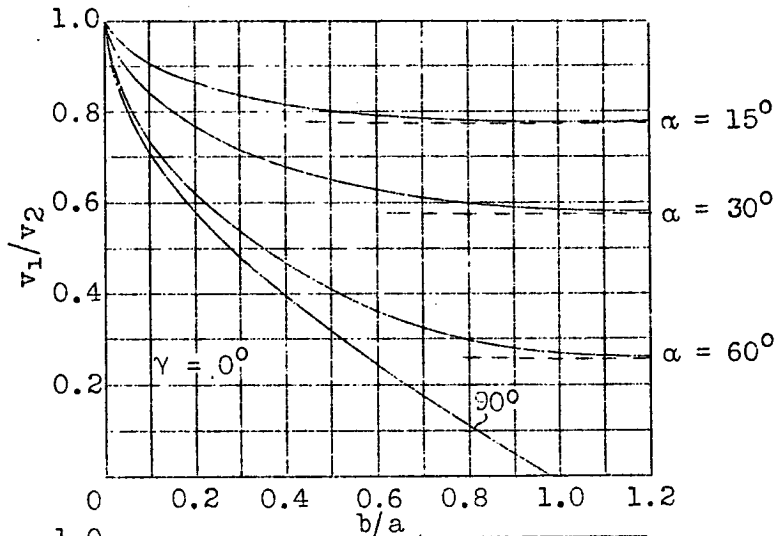


Fig.13

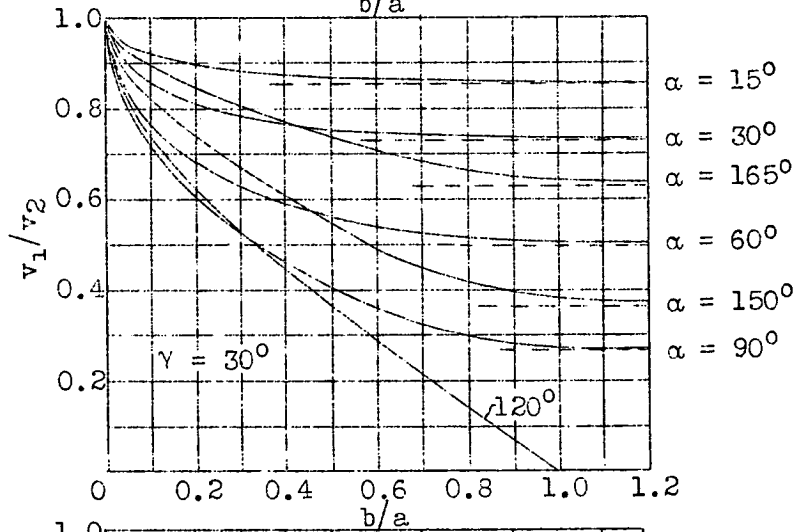
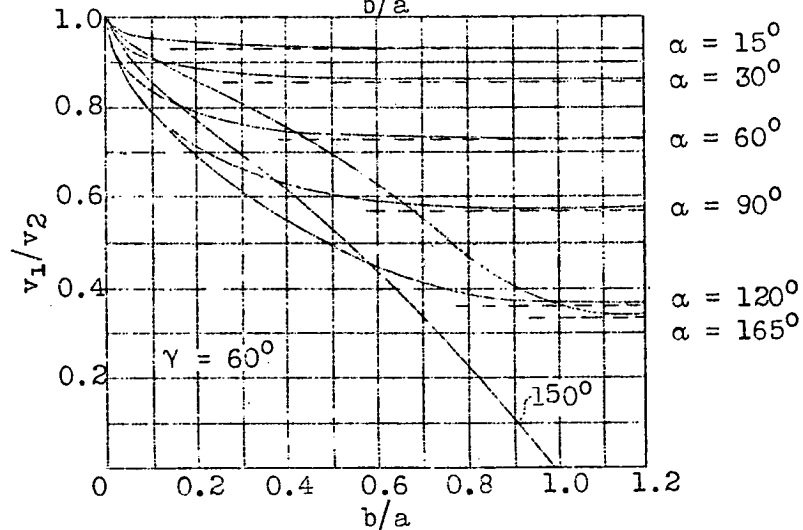
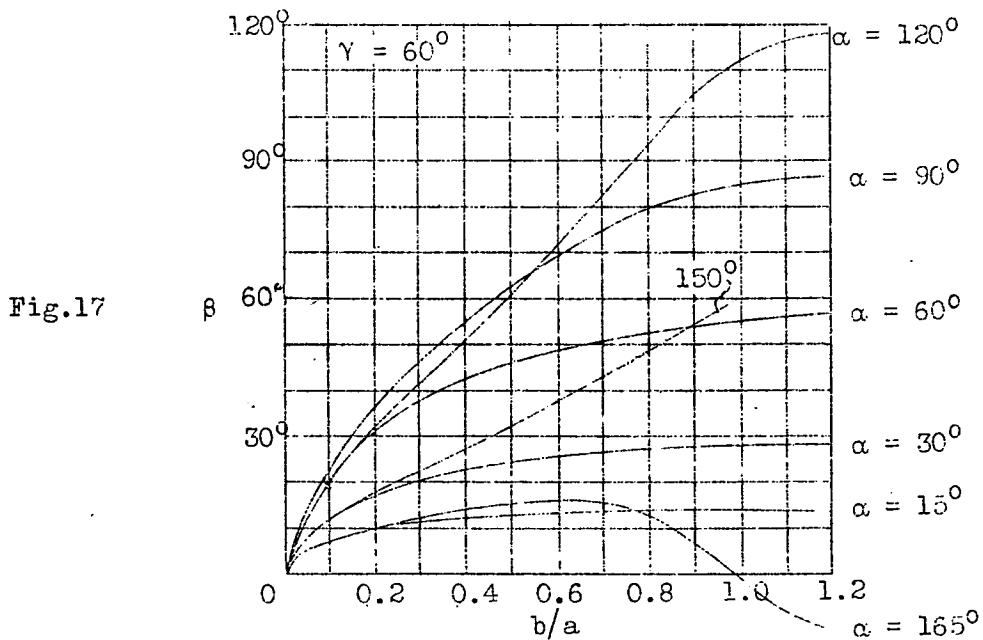
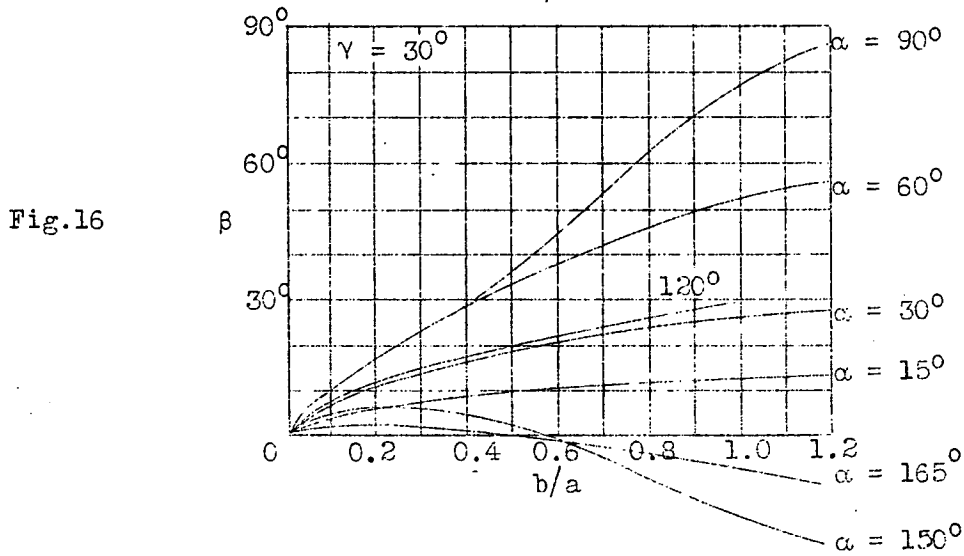
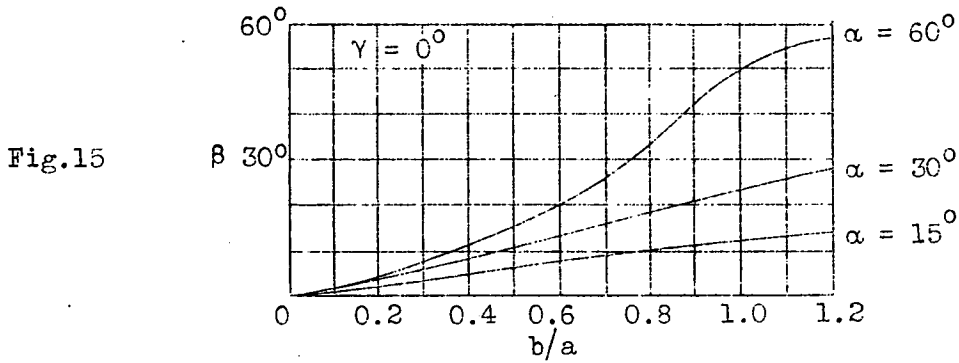


Fig.14



Figs.12,13,14 Ratio of velocities in front and behind screen, plotted against relative width of screen bars and angle of setting α for different slopes of flow γ . (Dashes = asymptotes)



Figs. 15,16,17 Angle of deflection β plotted against b/a and setting α for different slopes of flow γ .

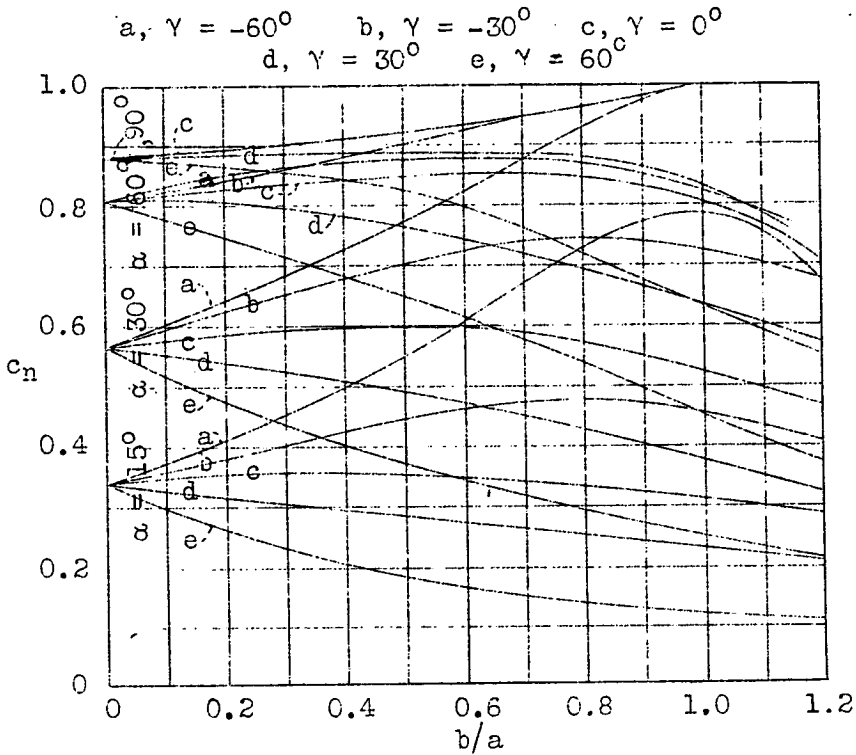


Fig.18 Normal force coefficient plotted against b/a , α and slope of flow γ .

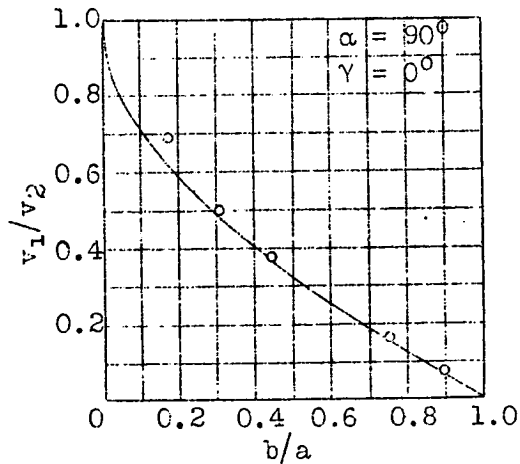


Fig.20 Ratio v_1/v_2 in front and behind screen by discharge of water in air through a flat screen. (Full line = theory)

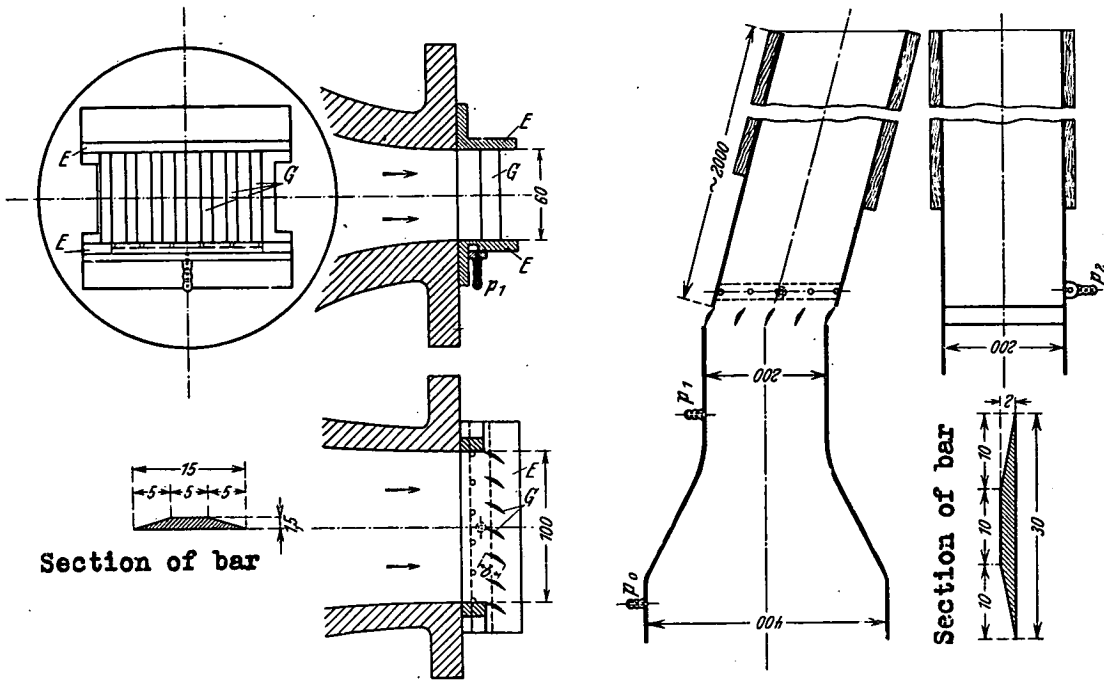


Fig.19 Experimental set-up for discharge of water in air.

Fig.23 Experimental set-up for discharge of air.

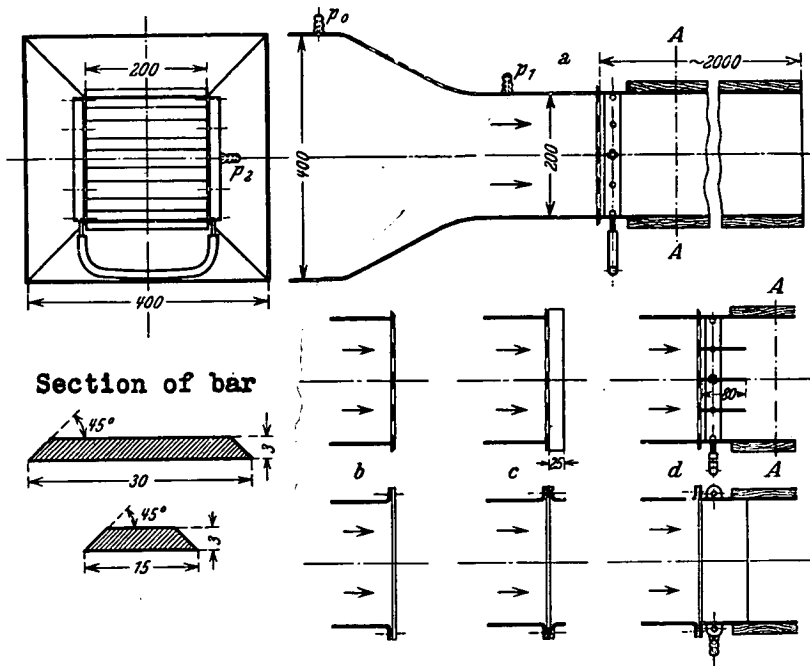


Fig.27 Various experimental arrangements for discharge of air from a flat screen.
 a, With discharge channel. b, Free discharge.
 c, With end plates. d, With channel and auxiliary bars.

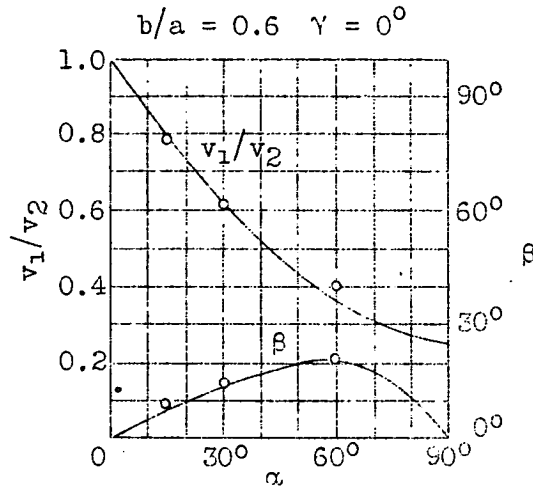
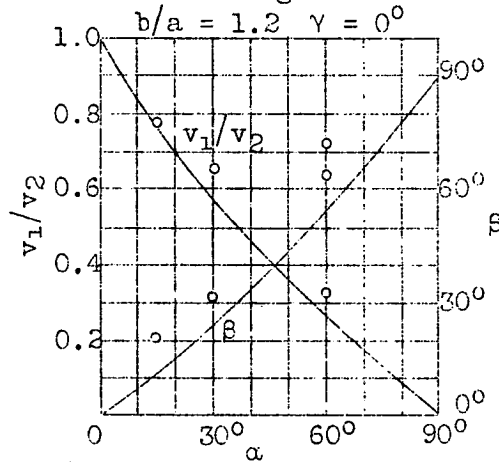


Fig.21



Figs.21,22 Ratio v_1/v_2 in front and behind screen upon discharging water in air for two relative bar widths. (Full curve = theory.)

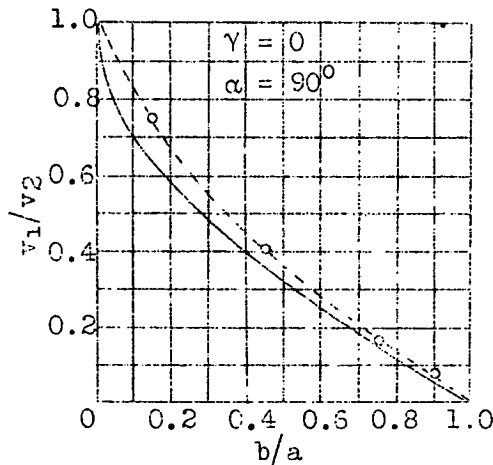


Fig.24 Ratio v_1/v_2 in front and behind screen by discharge of air through a flat screen. (Full line = theory), small screen no guide channel.

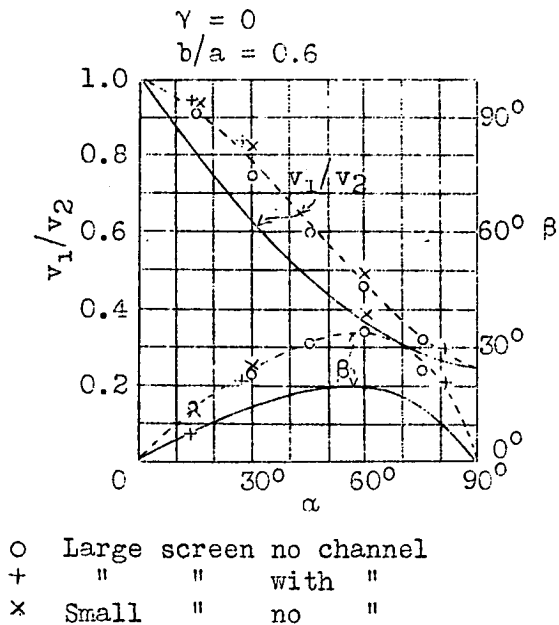


Fig.25

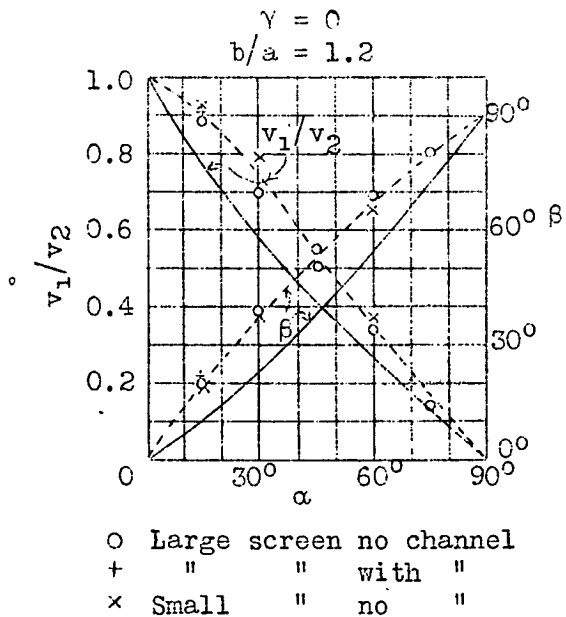


Fig.26

Figs.25,26 Ratio v_1/v_2 in front and behind screen by discharge of air for two b/a ratios. (Full line = theory.)

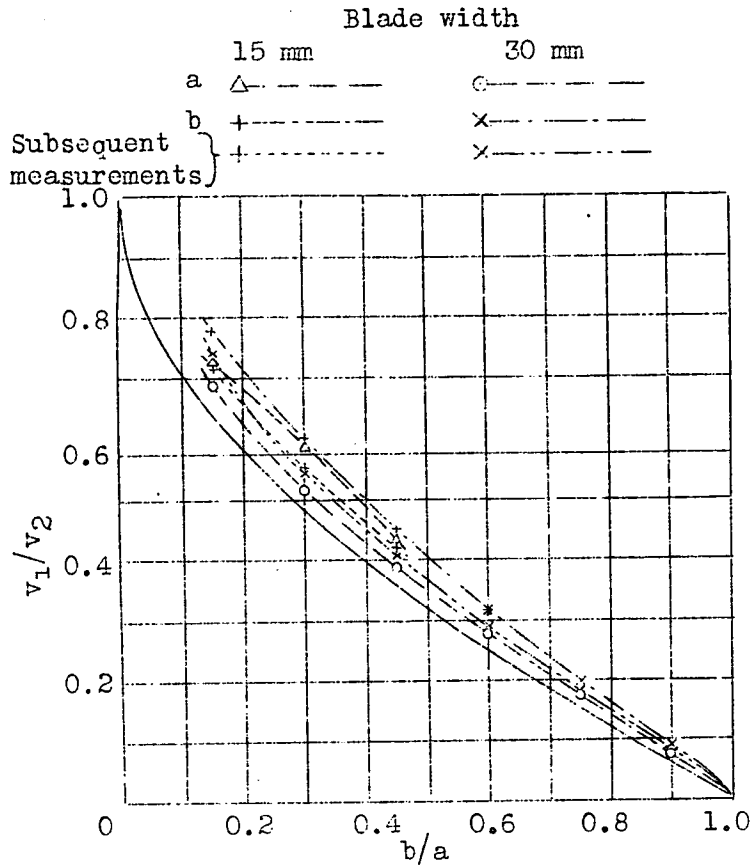


Fig.28

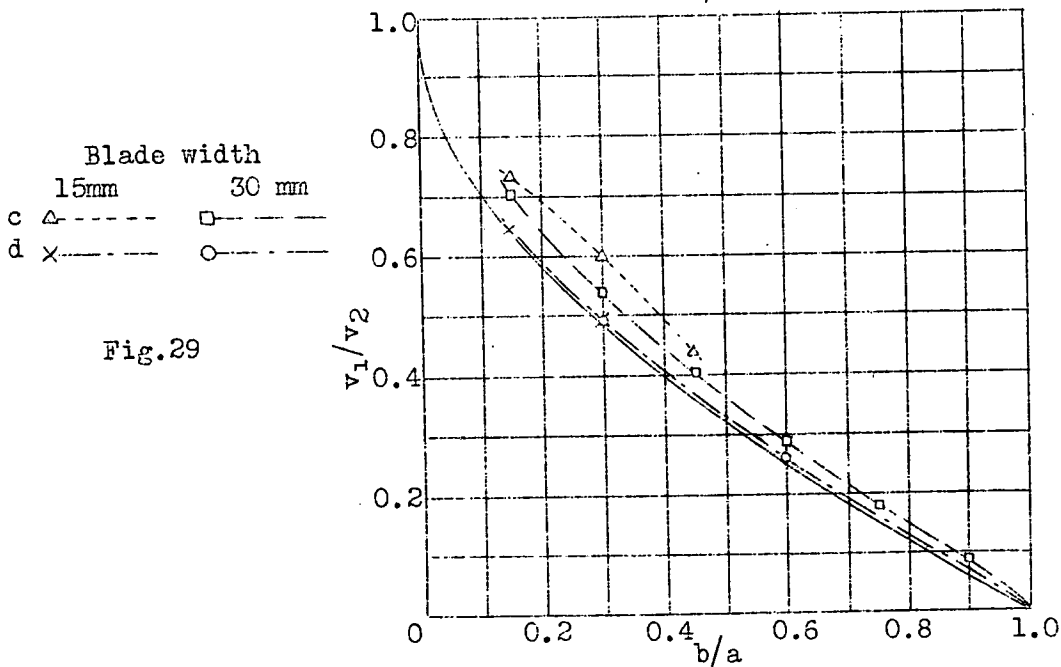


Fig.29

Figs.28,29 Results of tests with arrangements of figure 27.

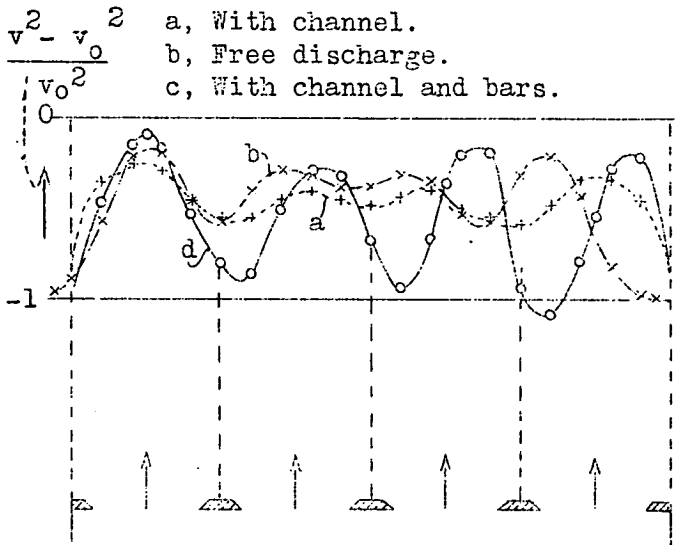


Fig.30 Energy distribution 13 cm back of screen with arrangements a, b and d of figure 27.

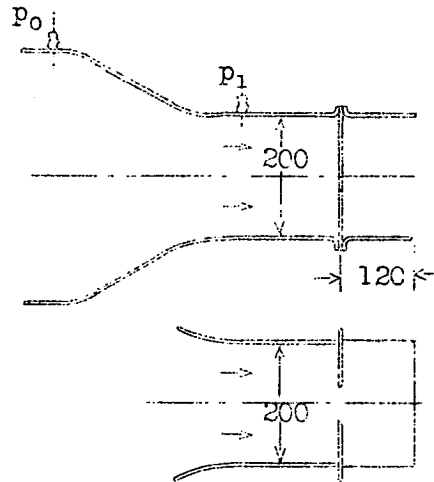


Fig.31 Experiments with one slot.

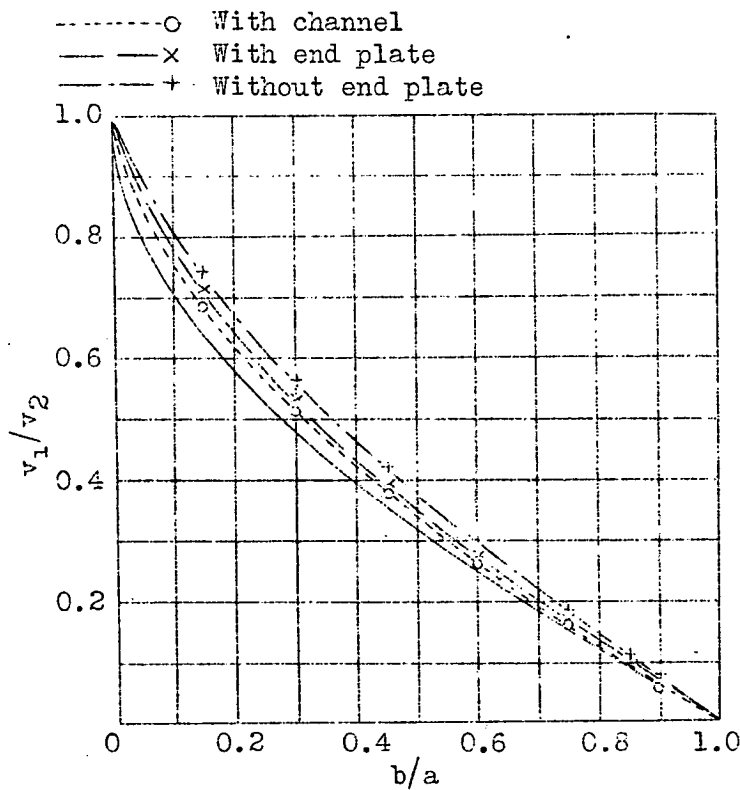


Fig.32 Results of tests with solitary slot.